ORIGINAL ARTICLE

Fabrication of 3D graphene anode for improving performance of miniaturized microbial fuel cells

Yuan Chen[1] · Zhiwei Zhao[1] · Songjie Li[1] · Boai Li[1] · Zhengjin Weng[1] · Yong Fang[1] · Wei Lei[1] · Helong Jiang[2]

Abstract

A three-dimensional graphene (3D GR) grown by chemical vapor deposition method was used as the anode of a miniaturized microbial fuel cell (mini-MFC), which was to be embedded in a 56-μL anode chamber for the formation of a thicker biofilm from *Shewanella* bacterial culture to promote high efficient extracellular electron transfer. Such 3D GR structure had fewer defects with few layers, and the framework showed significant high REDOX peak current density, high charge storage and low charge transfer resistance. Besides, the electron transport rate of 3D GR electrode was 0.0176 s^{-1}, which was about two times faster than that of GR electrode with nickel foam substrate (GR/NF). Benefiting from the macroporous networks, high electron transfer rate and electrocatalytic activity, 3D GR anode facilitated efficient mass transfer and effective electron transport, further forming denser biofilm on the 3D GR. The maximum output voltage and power density of this mini-MFC were 820 mV and 23.8 mW/m^2, which were much higher than those of the GR/NF anode at 590 mV and 12.8 mW/m^2 and the bare NF anode at 450 mV and 4.6 mW/m^2. The study demonstrated that 3D GR can be a promising anode material for improving MFC performance.

Keywords Biofilm · Electrocatalytic activity · Electron transfer · Redox reactions

Introduction

Industrial wastewater contains a large amount of organic matter, which belongs to renewable, low-polluting biomass energy (Rabaey and Verstraete 2005). As a green and recyclable technology that can recover this energy from wastewater and convert it into usable energy, microbial fuel cells (MFCs) can simultaneously solve the two key issues that affect human survival, energy shortage and environmental pollution (Logan et al. 2006; Bishoge et al. 2019). MFCs use electrochemically active bacteria as catalysts, and are an electrochemical system that uses the flow of electrons that occur during their metabolism to catalyze the redox reaction on the electrode surface (Li 2013). As a new type of clean energy that uses electroactive microorganisms to generate electricity, MFCs have not yet been applied on a large scale

(Kim et al. 2008; Flimban et al. 2018). The main obstacle restricting the commercialization and industrialization of MFCs is their low output power (Potter 1911).

The anode, as the carrier of electrochemically active bacteria (EAB) and the medium of electron transfer, is one of the main components of the microbial electrochemical system, and its performance directly determines the level of electricity produced by MFCs (Liu et al. 2004; Logan 2005). The ideal anode needs to have the following properties: Good biocompatibility, strong conductivity, large specific surface area, high porosity, rough surface, and many electrochemically active sites. Researchers at this stage have broadened and deepened the direction of anode transformation, from the application of conductive polymers to metal nanomaterials, from one-dimensional linear textiles to the construction of three-dimensional (3D) systems, and so on (Wei et al. 2011; He 2017). Thus, many efforts have been invested to fabricate the high-performance anode materials for large-scale applications of MFCs.

Carbon nanomaterials have stronger electrical conductivity and larger specific surface area and have been widely used to modify electrode materials in recent years. In particular, two-dimensional graphene (GR) materials have been

✉ Zhiwei Zhao
Zhao_zw@seu.edu.cn

1 School of Electronic Science and Engineering, Southeast University, Nanjing 210096, People's Republic of China

2 Institute of Geography and Limnology, Chinese Academy of Sciences, Nanjing 210096, People's Republic of China

widely used as electrode materials for charge output and storage because of their extremely fast electron mobility, ultra-high electrocatalytic activity and super-large specific surface area (Zhang and Liu 2010). Studies have shown that GR can promote the expression of signaling molecules by microorganisms, thus accelerating the growth of microorganisms and can be used as a medium molecule to improve the efficiency of electron transfer. Second, there are many fault structures on the surface of GR, which will add more reactive sites and electron transfer capacity generated by microbial oxidation metabolism to the electrode material itself. The special properties of GR materials make it have great potential in the application of anode materials for MFCs. Liu and colleagues deposited GR on the surface of carbon cloth by electrochemical deposition method, using *Pseudomonas aeruginosa* as an inoculum for the non-medium MFC (Liu et al. 2012). The modified GR electrode had a maximum power density of 52.5 mW/m^2, which was 2.7 times higher than the unmodified one (19.5 mW/m^2). Hou and colleagues used electrochemical method to reduce GR oxide (ERGNO) and coated with polyaniline (PANI) nanofibers on the surface of carbon cloth to prepare a new type of MFC anode (Hou et al. 2013). After combining the advantages of the two, with PANI-ERGNO/carbon cloth as the anode, the maximum power density could reach 1390 mW/m^2, which was 3 times that of the control carbon cloth electrode. In the application of MFC, the two-dimensional GR material is usually modified on the surface of the substrate material, such as carbon cloth, carbon paper, graphite block and so on. The introduction of GR did greatly reduce the resistance to electron transfer, strengthened the close connection between bacteria and electrodes, and improved the efficiency of electricity generation of MFC, but it did not increase the efficiency of enrichment of microorganisms in electrode materials.

Compared to two-dimensional GR materials, 3D GR is simpler to form porous 3D layered structures (Zhang et al. 2011). Thus, it is a very ideal MFC anode material. Yang and colleagues reported a 3D nitrogen-doped GR aerogel (N-GA) as an anode material for MFCs by hydrothermal reaction and freeze-dry method (Yang et al. 2016). Importantly, the dual-chamber milliliter-scale MFC with N-GA anode yielded an outstanding volumetric power density of 225 ± 12 W/m^3 normalized to the total volume of the anodic chamber (750 ± 40 W/m^3 normalized to the volume of the anode). Chen and colleagues developed a reduced GR oxide/polyacrylamide (rGO/PAM) 3D composite hydrogel coupled with current collector graphite brush (GB) as anode for MFCs, which produced a remarkably high maximum power density and volumetric power density of 758 mW/m^2 and 53 W/m^3, respectively (Chen et al. 2019). The 3D graphene aerogels reported in previous work were usually prepared with GO as the precursor under the conditions of rapid freezing of liquid nitrogen. However, due to the strong π–π interaction force between GO lamellas, the overlap and agglomeration between the lamellas resulted in the decrease of the number of effective GA channels, significantly narrowing the effective surface area for bacterial attachment. In addition, the pore size of 3D graphene aerogel was usually distributed between 2 and 100 nm, and the size of microorganisms was generally 1–2 μm, so it was easy to block the pores of 3D GR aerogel. To solve this problem, existing research has introduced intercalation materials into the precursor such as multi-walled carbon nanotubes and metal oxides, but they will increase the complexity and cost of electrode manufacturing.

MFCs can be divided into two-chamber MFCs, single-chamber MFCs and "three-in-one" MFCs, depending on their assembly method and structure. A proton exchange membrane (PEM) separates the anode and cathode chambers. However, this configuration is difficult to scale-up due to the high cost of the PEM. Single-chamber MFCs are easy to scale up, but their performance is still not adequate for practical applications. Additionally, the size of the cell has a significant impact on performance. Small or miniaturized MFCs (mini-MFCs) are preferred by researchers since large MFCs are frequently constrained in practice due to their size and lack of power. Mini-MFCs are smaller, have shorter distances between electrodes, lower resistance and easier electron transfer.

In the present study, a 3D macroporous GR was developed and employed as anode in miniaturized MFCs (mini-MFC). This type of 3D macroporous GR framework showed significant high capacitance current, high charge storage, low charge transfer resistance and rendered the inner surface of anode accessible for bacterial adhesion, compared with GR with nickel foam substrate (GR/NF) and the bare nickel foam (NF) materials in this study. Mini-MFCs equipped with 3D GR anodes were compared to assess the effect of different anodes on mini-MFC performance and biofilm community structure. The aim of the present work was to evaluate the performance of a 3D macroporous GR structured anode in mini-MFCs inoculated with *Shewanella oneidensis* MR-1 and the electron transfer mechanism between anode and electrochemically active bacteria will also be presented.

Materials and methods

Synthesis of 3D GR anode

3D GR was synthesized by CVD (CVD3-8-12, CINITE Corp., Beijing, China) using foamed nickel as the matrix and methane as the carbon source. The specific process flow was as follows: Foamed nickel (area density was about 320 gm^{-2}, thickness was about 1 mm) was used as a 3D

scaffold template, and they were cut into 30×10 mm pieces. At a temperature of 1000 °C in a 1200 °C open type double temperature zone tube furnace (OTF-1200X-II), carbon was introduced into the nickel foam by decomposing CH_4, and then GR films were deposited on the surface of the nickel foam. The flow rate of methane gas is 10 sccm and the synthesis duration was 10 min. In order to remove the nickel foam, the 3D GR network was first coated with polymethyl methacrylate (PMMA), and then the 3D GR sample coated with the PMMA film was placed in a 0.3 mol/L ferric chloride solution to corrode and remove the NF substrate. Finally, the sample was placed in acetone to remove the PMMA film. A complete GR with a 3D network structure was obtained. The preparation of GR/NF eliminated the step of etching the substrate.

Characterization of the anode materials

The surface morphology of 3D GR was mainly observed by scanning electron microscopy (SEM Quanta 200, FEI Corp., US), and its quality and layer number were analyzed by Raman spectroscopy. The Raman spectrometer was the Labram HR800 manufactured by Jobin Yvon Company in France. Its spectral range was 300–1000 nm, and the resolution was neon (585.25 nm): better than 3 cm^{-1}. The electrochemical properties of the samples were studied by cyclic voltammetry (CV) and electrochemical impedance spectroscopy (EIS) at the Electrochemical Workstation, in which the scanning voltage range was from − 1 to 1.5 V with the scanning speed of 20–360 mV. The setting frequency range of EIS was from 0.1 to 100 k Hz, and the disturbance signal was 5 mV. The electrolyte for CV and EIS measurements was consisting of 50 mL of 2 mol/L NaOH solution.

Mini-MFC setup and measurement

A single-chamber mini-MFC was fabricated for anode performance evaluation. The anode chamber had a volume of 56 μL, the 3D GR, GR/NF and the pure NF were used as the anode, respectively. The anode chamber was made of polydimethylsiloxane (PDMS), which was non-toxic, odorless and had good chemical stability. Nafion 117 membrane was selected for proton exchange membrane. Before using, the Nafion membrane was immersed in 2% H_2O_2 solution and 1% NaOH solution successively and boiled for 1 h, respectively. Then Pt/C catalyst was coated on one side of Nafion membrane. The anode chambers were inoculated with *Shewanella oneidensis* MR-1. Anolyte consisted of 1.3608 g/L of NaCH$_3$COO, 2.5 g/L of NaHCO$_3$, 0.1 g/L of KCl, 1.5 g/L of NH$_4$Cl, 0.6 g/L of NaH$_2$PO$_4$·2H$_2$O, 0.1 g/L of CaCl$_2$·2H$_2$O, 1 mL/L of Vitamins and 1 mL/L of trace elements.

The performance of MFCs were evaluated by measuring the voltage curve, polarization curve and power density curve. All experiments were carried out at a constant temperature of 25 °C. The output voltage test of MFC was automatically recorded and stored by voltage signal acquisition system. When microorganisms were enriched on the surface of the anode, the voltage of MFCs slowly increased and reached the maximum value that was called the open circuit voltage (OCV). The OCV reflected the discharge capacity of the MFC and could also be understood as the output load voltage when the circuit was disconnected. After the voltage of the mini-MFC reached stability, changed the resistance value of the external resistance of the cell and measured the resistance voltage. According to Ohm's law (1), the current density could be obtained as follows:

$$i = \frac{U}{RS}, \tag{1}$$

where U is the resistance voltage, R is the external resistance, and S is the area of the mini-MFC electrode. According to the current density, the polarization curve could be obtained.

The power density curve represents the relationship between power density and current density, and the power (P) per unit area could be obtained through formula (2).

$$P = UI = \frac{U^2}{RS}, \tag{2}$$

where U is the mini-MFC voltage, R is the external resistance and S is the anode area of the mini-MFC.

Results and discussion

Morphological and electrochemical characteristics of 3D GR

Surface morphology of 3D GR could be obtained by SEM. The sample preparation process consisted of disassembling the mini-MFC with 3D GR as the anode, removing the anode, submerging it in a solution of 2.5% glutaraldehyde (pH = 6.8) and placing it in a refrigerator at 4 °C for 24 h. The samples were then washed three times using a phosphate buffer solution (pH = 6.8), soaking for 10–15 min each time. The samples were then dehydrated with successive gradients of ethanol concentration (30%, 50%, 70%, 80%, 95%), each step lasting 15–20 min. Finally, the samples were allowed to dry and the subsequent SEM procedure was carried out as for normal samples. Figure 1 shows SEM images of 3D GR with different magnification. Obviously, in Fig. 1a, surface morphology of 3D GR were consistent with those of NF substrate in
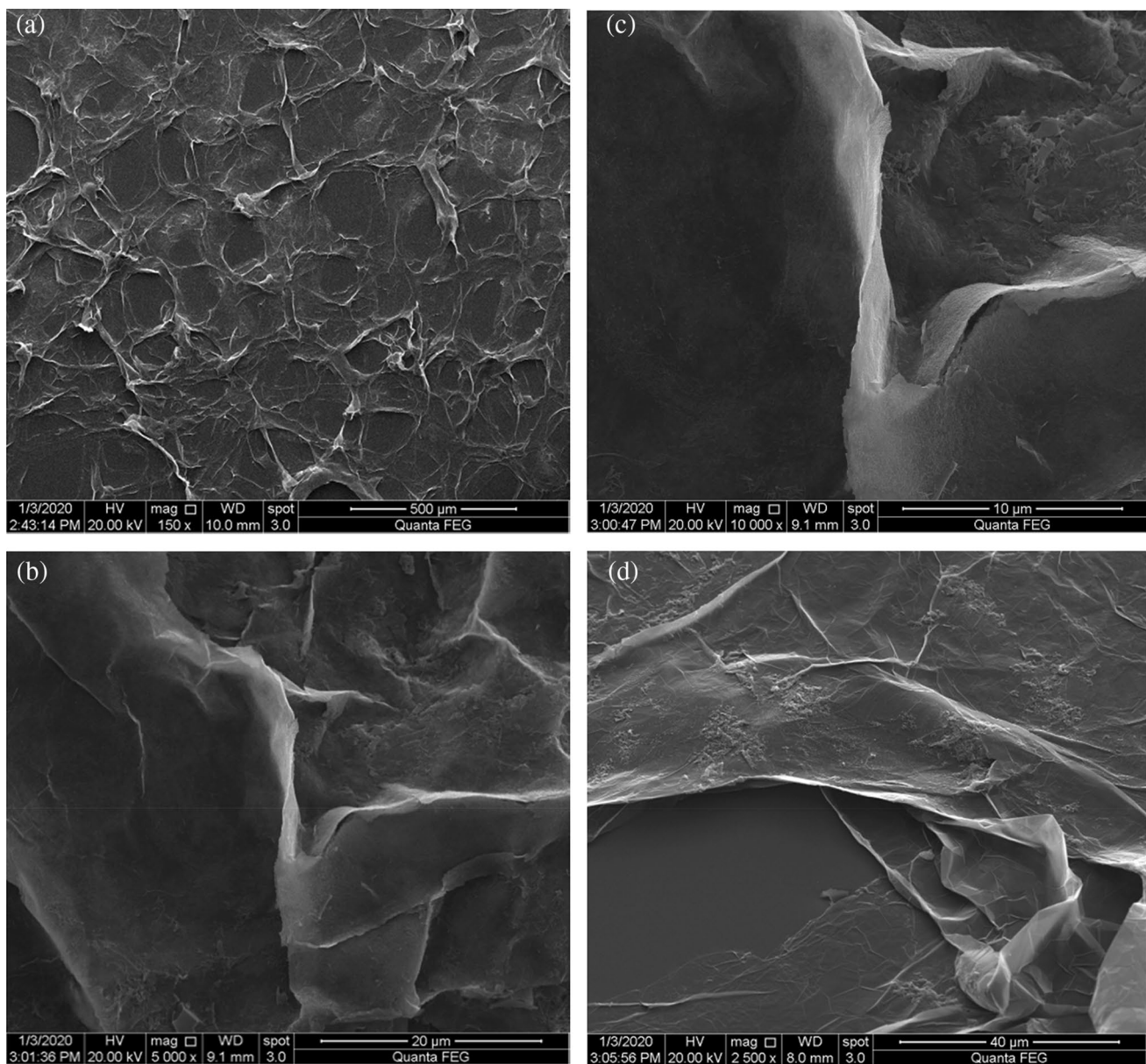
Fig. 1 SEM images of 3D GR at ×150 (**a**), ×5000 (**b**), ×10,000 (**c**), ×2500 (**d**) magnifications

terms of shape and size of the pores. The pore size of 3D GR was about 100–200 μm that ensured unimpeded transport of the matrix, where bacteria (usually in the range of 1–2 μm) could easily spread and colonize on both exterior and interior surfaces of 3D GR anodes (Hou et al. 2013). In comparison to currently available nanomaterial-coated electrodes with higher specific surface areas, the 3D GR prepared here promotes superior bacterial adhesion and growth. After etching the substrate, the 3D GR presented a surface morphology of multiple folds and sheets (Fig. 1b–d), which had resulted from the hydrogen produced by the reaction of the acid with the NF during the

etching of the NF, resulting in defects to the surface and edges of the 3D GR.

As a useful and non-destructive technique, Raman spectroscopy with a laser excitation wavelength of 532 nm was used to characterize defects and layers in GR with the presence of ordered and disordered structures (Dato et al. 2008). Figure 2a shows the Raman spectrum of the 3D GR prepared by CVD. The 3D GR was placed on a PDMS substrate for testing. Obviously, the G peak of the 3D GR sample is at 1584.5 cm^{-1}, which was caused by the in-plane vibration of the carbon atom sp^2 and usually appeared near 1580 cm^{-1} (Ferrari 2007). The appearance of 2D peak at 2709.4 cm^{-1}
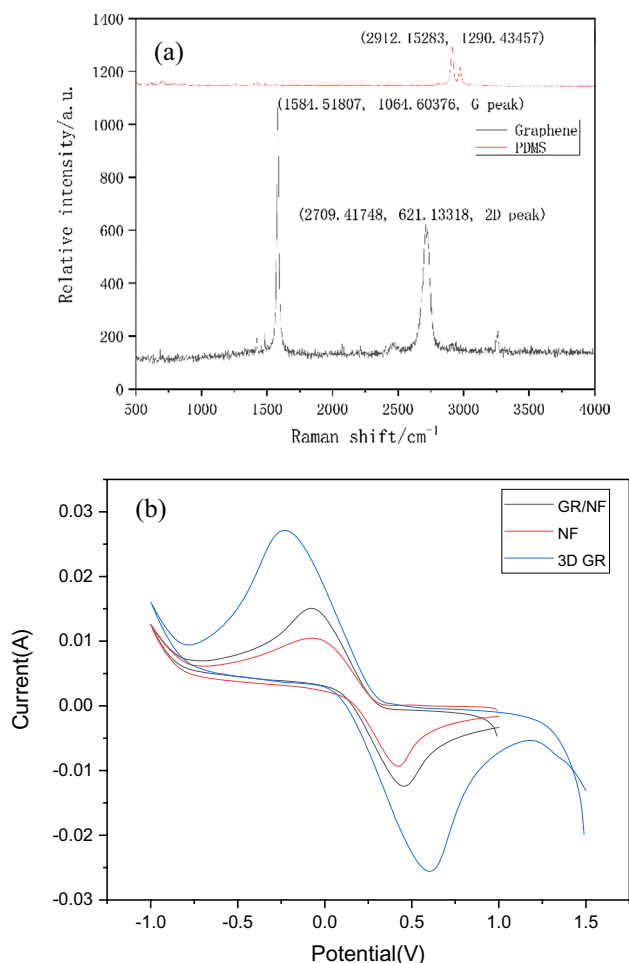
Fig. 2 Raman spectroscopy of 3D GR (**a**) and CV Curves of 3D GR, GR/NF and NF at the scanning speed of 50 mV/s (**b**)

was a second-order Raman peak with two-phonon resonance, which was used to characterize the interlayer stacking mode of carbon atoms in GR samples (Zhu et al. 2010). In Raman spectroscopy, the average number of GR layers could be estimated based on the 2D/G peak ratio. The calculated 2D/G peak ratio was about 0.58, indicating few-layer of 3D GR obtained by CVD using NF as the templates. Interestingly, in Raman spectrum, no obvious observed D peak suggests that there are fewer defects in the 3D GR sample obtained by the CVD method using foamed nickel as the matrix and methane as the carbon source.

CV was used to evaluate the electrochemical properties of 3D GR, GR/NF and NF materials. The Redox peak of CV curve of electrode materials was observed to examine the Redox reaction and reversibility of materials. As shown in Fig. 2b, a pair of clear Redox peaks could be observed on each anode. Obviously, both the oxidation and reduction peak currents on the 3D GR electrode were significantly enhanced compared with the exposed NF and the GR/NF. At the same time, it was found that the potential difference

between the oxidation peak and reduction peak of 3D GR was 112 mV, which was the largest among the three samples. The high separation degree of the oxidation peak and reduction peak was caused by the roughness and specific surface area of the electrode surface (Ramasamy et al. 2008). The region included in the CV curve of 3D GR (Fig. 2b) indicated the charge storage capacity on the surface of the electrode and the higher electrocatalytic location (Peng et al. 2013). Compared with the other two electrodes, 3D GR had the highest current and the largest closure area, indicating that 3D GR had better capacitance performance.

Figure 3a, b shows CV curves of 3D GR and GR/NF when the scanning rate was increased from 20 to 360 mV. As the scanning rate increased, the peak current density of each electrode increased, and along with the positive direction of the oxidation peak shift, and the negative direction of the reduction peak shift. According to the CV diagram of different scanning rates, the reaction kinetic rate constant Ks of the surface reactions of 3D GR electrode materials could be calculated by using the Laviron model, which was used to measure the electron transport rate of 3D GR (Laviron 1979). According to the Laviron model, the relationship between peak potential and scanning rate follows the following formula (3), in which α, v and E^σ are the conversion factor (between 0 and 1), the scanning rate and the type potential, respectively. E_{pa} is the oxidation peak potential, E_{pc} is the reduction peak potential, and everything else is constant.

$$
\begin{aligned}
E_{pa} &= Eo\prime + \frac{RT}{(1-\alpha)nF} \ln \frac{(1-\alpha)nF}{RTk_s} + \frac{RT}{(1-\alpha)nF} \ln v E_{pc} \\
&= Eo\prime + \frac{RT}{\alpha nF} \ln \frac{RTk_s}{\alpha nF} - \frac{RT}{\alpha nF} \ln v
\end{aligned}
\tag{3}
$$

By reading the potential voltage value of the oxidation peak current and reduction peak current at each scanning rate in the figure, and subbing it into Eq. (3), the electron transport rate Ks could be derived. A curve graph of the relationship between the scanning rate and the redox peak voltage value of 3D GR and GR/NF was drawn, as shown in Fig. 3c, d. According to the linear relationship of the above two materials between E_p and $\ln v$, the K_s value for GR/NF was derived to be 0.0087 s^{-1}, and for 3D GR, it was as high as 0.0176 s^{-1}. Such K_s value for 3D GR was almost two times higher than that for GR/NF, indicating the more efficient electrons transfer that flow through the solution and the electrode surface.

The electrochemical properties of 3D GR, GR/NF and NF electrode materials were further compared and analyzed by EIS, as shown in Fig. 3e. EIS map consists of the semicircular part of the reaction charge transfer at high frequency and the linear part of the reaction solution property at low
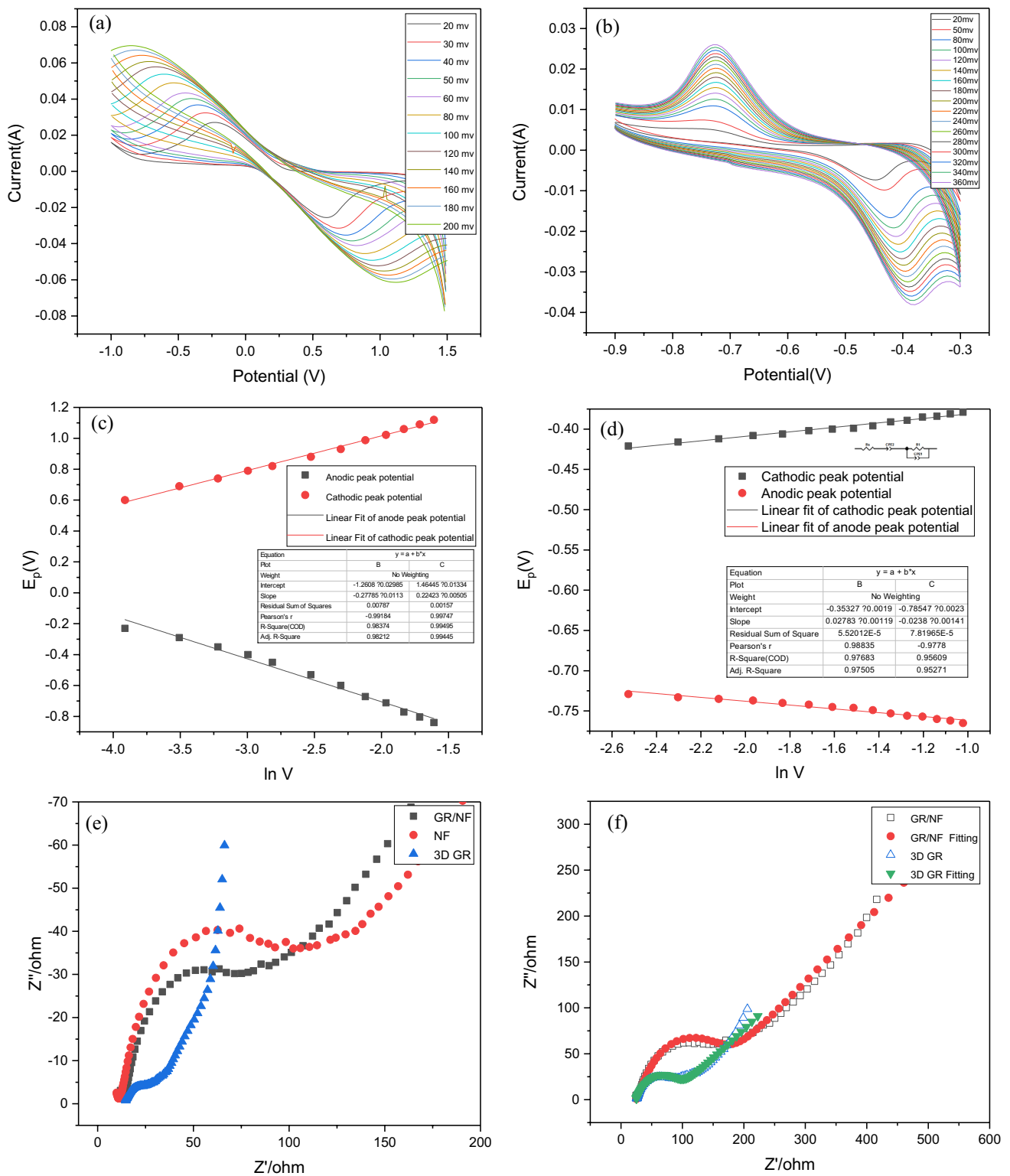
Fig. 3 CV curves of 3D GR (**a**) and GR/NF (**b**) at scanning speed of 20–360 mV; E_p and Inv diagrams of 3D GR (**c**) and GR/NF (**d**); EIS curves of 3D GR, GR/NF and NF (**e**); EIS fitting diagrams of 3D GR and GR/NF (**f**)

frequency. The real axial intercept of the three samples at the starting point of high frequency was similar, indicating the similar solution resistance value (Rs). 3D GR had the smallest semicircle diameter in the high-frequency region, while NF had the largest. The diameter of the semicircle corresponded to the interfacial charge transfer resistance (Rct), which meant that the surface of 3D GR material had the strongest electron transfer ability. In addition, the Rct of GR/NF was larger than that of 3D GR because of the presence of NF, the electron transfer performance of the surface of NF material was far inferior to that of 3D GR material.

The EIS data in Fig. 3f were fitted through the equivalent circuit. The Zview program was used to fit the Nyquist plots to get the values of each parameter. Since the 3D GR and the GR/NF were tested in the same solution and the position of the working electrode was consistent with the relative position of the counter electrode and the reference electrode, the Rs parameters of the two materials were basically the same. The charge transfer resistance (Rct) of the 3D GR material was 30.94 Ωcm^{-2}, which was significantly smaller than that of GR/NF (38.87 Ωcm^{-2}), indicating that the electrical conductivity of 3D GR had been significantly improved after combining the structural advantages of 3D NF framework. The outstanding reduction of Rct for 3D GR electrode indicated that 3D GR achieved considerably a faster electrochemical reaction and reduced the electron transfer resistance between the electrode and electrolyte.
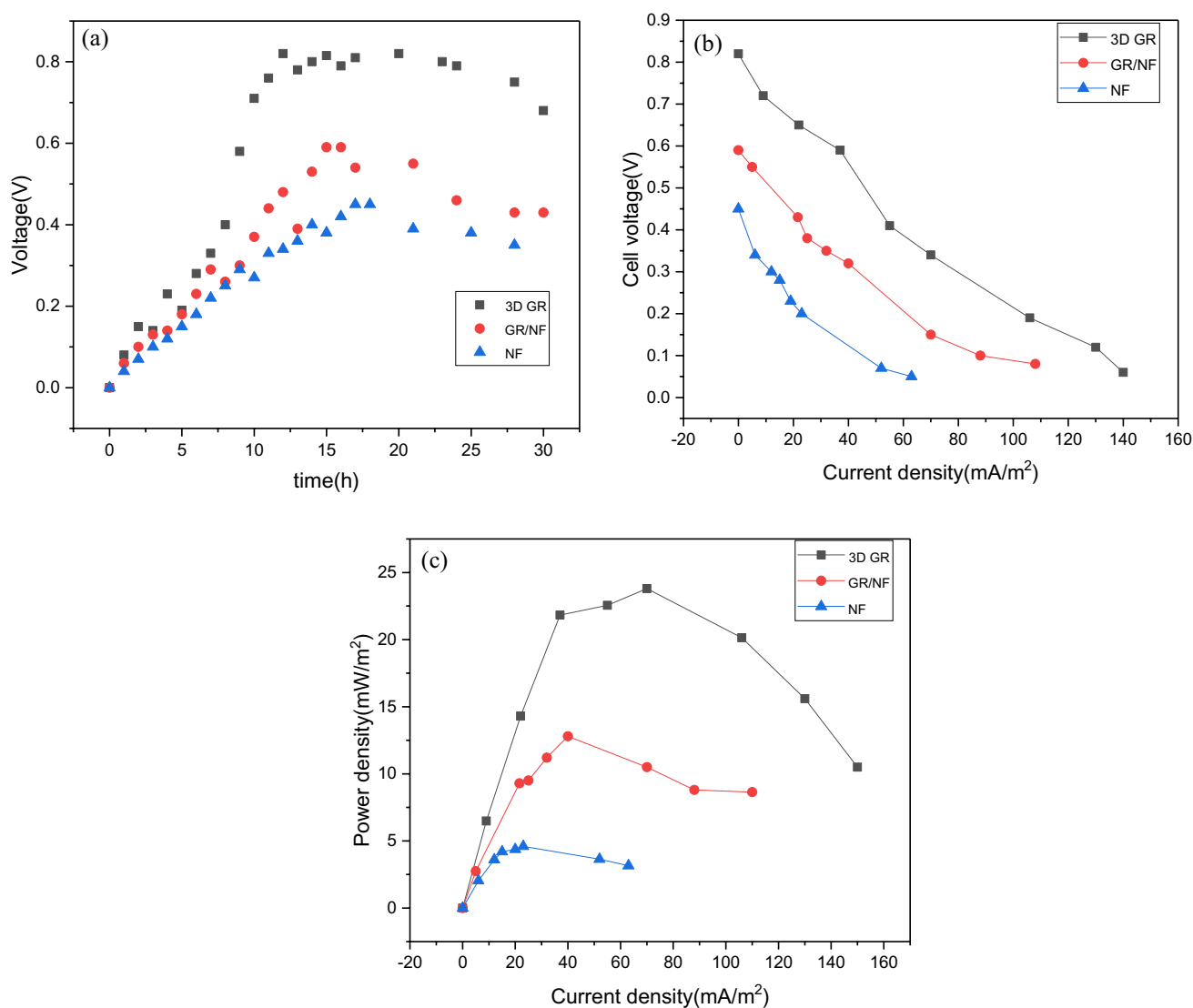

Fig. 4 Output voltage acquisition curves (**a**), polarization curves (**b**) and power density curves (**c**) of mini-MFC with 3D GR, GR/NF and NF as anode

Mini-MFC performances with different anodes

Three kinds of mini-MFCs were constructed by using 3D GR, GR/NF and NF as anodes, respectively. The performance of these mini-MFCs were recorded simultaneously with an external resistance of 1000 kΩ. As shown in Fig. 4a, at the beginning of operation, the mini-MFC voltage of different anodes rose slowly and the difference was not obvious. After 7 h' operating, the mini-MFC output voltage with 3D GR anode rose significantly faster than that of the other two anodes, which tended to be stable with longer operating hours.

The OCV of the 3D GR anode was 0.82 V, which was larger than that of the GR/NF anode (0.59 V) and the NF anode (0.45 V). Mini-MFC with 3D GR anode could achieve the shortest start-up time and the highest open circuit voltage, which implied that the higher electrogenic activity of the anode and higher reaction rate in the anode chamber. During the process, all parameters were kept the same except for the anode material type. The different variation in OCV could be attributed to the performance of the anode with different materials.

When the mini-MFC voltage reached the maximum and tended to be stable, the polarization curve and power density curve of the battery were tested by connecting different resistance values from 1000 to 10 kΩ. It could be seen from Fig. 4b that the mini-MFC output voltage of 3D GR anode decreased more slowly with the decrease of external load compared with that of NF anode and GR/NF anode. The slope of the polarization curve with 3D GR anode was the smallest, indicating that the less the internal resistance of this MFC the faster the electron transfer process. This showed that 3D GR was preferred to the NF and GR/NF electrode materials for the anode of MFC.

The maximum power density of the mini-MFC with the 3D GR anode in Fig. 4c reached 23.8 mW/m^2, which was 1.8 and 5.2 times higher than that of the MFCs with GR/NF anode and the bare NF anode, respectively (Liu et al. 2012). Although the conductivity of 3D metal electrodes such as NF and stainless-steel mesh was high, the biocompatibility and chemical stability were poor, which was not conducive to the adhesion of microorganisms and was prone to corrosion and passivation in the long-term operation of the microbial electrochemical system. While the 3D GR after etching the substrate retained the 3D porous structure that was conducive to bacterial adhesion, the advantages of GR's ultra-high conductivity and better biocompatibility had been fully amplified, and it could allow thicker external electric biofilm growth that minimized the transfer of ineffective electrons from microorganisms that was far away from the anode. When there was more effective electron transfer on the biofilm and more current transfer, the output power density of MFC became better.

Investigation of anode biofilms

SEM analysis on the anodes inoculated with bacteria provided evidence that a large number of *Shewanella* accumulate in the 3D GR framework and adhere to each other to form a thicker biofilm (Fig. 5a, b), indicating that the 3D structure of GR could promote the adhesion of bacteria on the anode, which played a key role in improving the power output of MFC. In contrast to the high bacterial loading on both external and internal surfaces of the 3D GR anode, the GR/NF was coated with much fewer bacterial cells, further confirming the poor biocompatibility of NF (Fig. 5d). In addition, the morphology of microbial nanowires observed between the microorganism and the electrode surface (Fig. 5c) suggested that electrons might be quantitatively transferred to the anode by Redox proteins on the bacterial surface through the bacterial nanowires. Therefore, the 3D macroporous structure and the high affinity between *S. oneidensis* MR-1 and GR promoted the bacterial loading capacity of 3D GR anode, which eventually contributed to the high performance of mini-MFC with 3D GR anode.

Conclusions

This study reports a mini-MFC with a 3D GR anode capable of accommodating a high population of microbes. The large pore structure of 3D GR with the pore size of 100–200 μm enlarged the surface area for bacterial loading and colonization in the anode interior, and ensured unimpeded transport of the matrix. Benefiting from the macroporous networks, high electron transfer rate and electrocatalytic activity, 3D GR anode facilitated efficient mass transfer and effective electron transport, further forming denser biofilm on the outside and inside of the 3D GR. Consequently, the maximum output voltage and the maximum power density of the 3D GR anode was 820 mV and 23.8 mW/m^2, which was 1.8 and 5.2 times higher than that of the MFCs with GR/NF anode and the bare NF anode, respectively. The present study demonstrated that 3D GR can be a promising anode material for improving MFC performance.
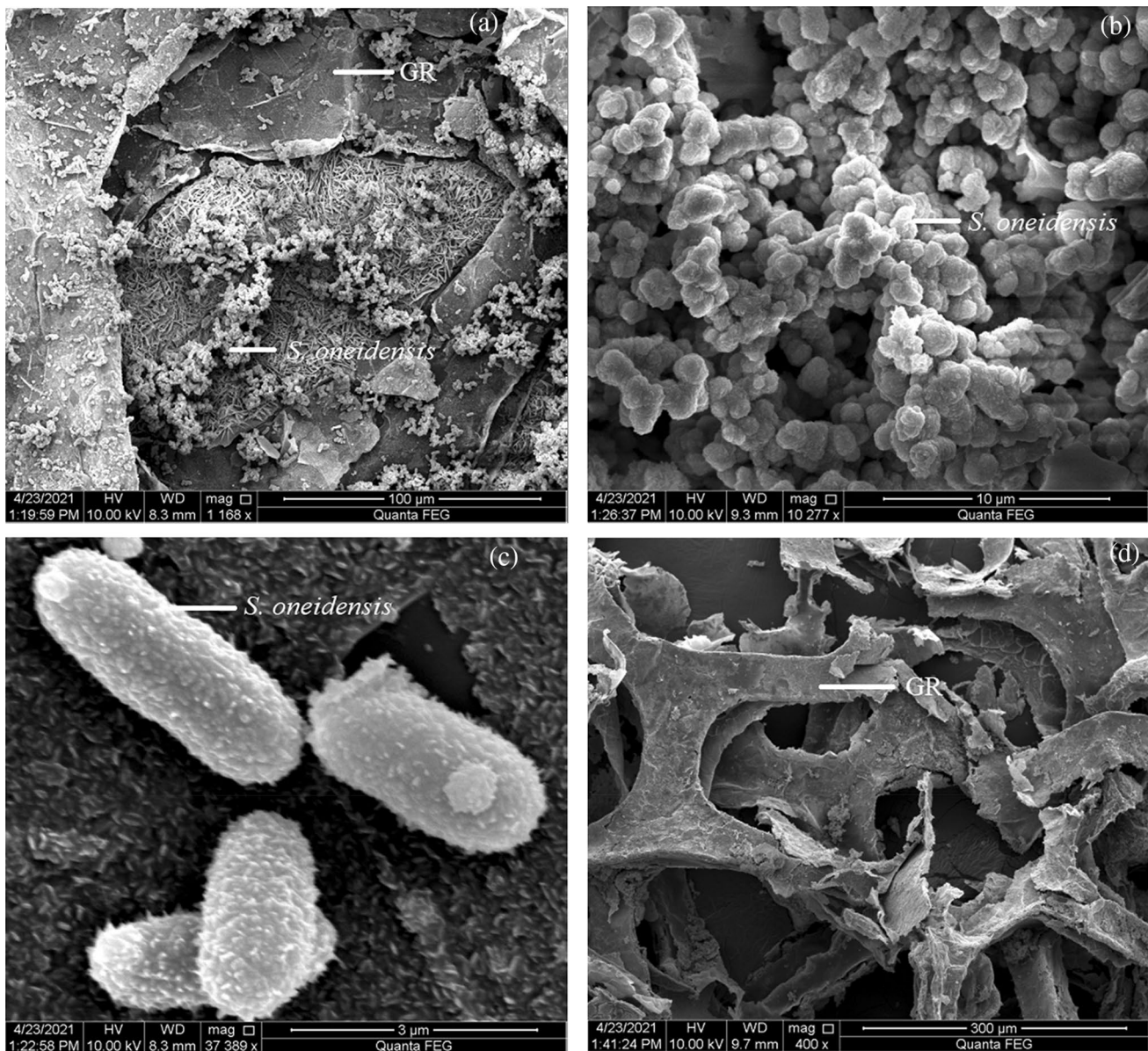
Fig. 5 SEM images of bacteria formed on the 3D GR (**a**–**c**) anodes and GR/NF (**d**)

References

Bishoge OK, Zhang L, Mushi WG (2019) The potential renewable energy for sustainable development in Tanzania: a review. Clean Technol 1(1):70–88. https://doi.org/10.3390/cleantechnol101 0006

Chen JY, Xie P, Zhang ZP (2019) Reduced graphene oxide/polyacrylamide composite hydrogel scaffold as biocompatible anode for microbial fuel cell. Chem Eng J 361:615–624. https://doi.org/10.1016/j.cej.2018.12.116

Dato A, Radmilovic V, Lee Z, Phillips J, Frenklach M (2008) Substrate-free gas-phase synthesis of graphene sheets. Nano Lett 8(7):2012–2016. https://doi.org/10.1021/nl8011566

Ferrari AC (2007) Raman spectroscopy of graphene and graphite: disorder, electron–phonon coupling, doping and nonadiabatic effects. Solid State Commun 143(1–2):47–57. https://doi.org/10.1016/j.ssc.2007.03.052

Flimban SG, Kim T, Ismail IMI, Oh S-E (2018) Overview of microbial fuel cell (MFC) recent advancement from fundamentals to applications: MFC designs, major elements, and scalability. Preprints. https://doi.org/10.20944/preprints201810.0763.v1

He Z (2017) Development of microbial fuel cells needs to go beyond "power density." ACS Energy Lett 2(3):700–702. https://doi.org/10.1021/acsenergylett.7b00041

Hou JX, Liu ZL, Zhang PY (2013) A new method for fabrication of graphene/polyaniline nanocomplex modified microbial fuel cell anodes. J Power Sources 224:139–144. https://doi.org/10.1016/j.jpowsour.2012.09.091

Kim I-S, Chae K-J, Choi M-J, Verstraete W (2008) Microbial fuel cells: recent advances, bacterial communities and application beyond electricity generation. Environ Eng Res 13(2):51–65. https://doi.org/10.4491/eer.2008.13.2.051

Laviron E (1979) General expression of the linear potential sweep voltammogram in the case of diffusionless electrochemical systems. J Electroanal Chem 101(1):19–28. https://doi.org/10.1016/S0022-0728(79)80075-3

Li Y (2013) The current response of a mediated biological fuel cell with acinetobacter calcoaceticus: the role of mediator adsorption and reduction kinetics. Univ Canterb Chem Process Eng. https://doi.org/10.26021/2766

Liu H, Ramnarayanan R, Logan BE (2004) Production of electricity during wastewater treatment using a single chamber microbial fuel cell. Environ Sci Technol 38(7):2281–2285. https://doi.org/10.1021/es034923g

Liu J, Qiao Y, Guo CX, Lim S, Song H, Li CM (2012) Graphene/carbon cloth anode for high-performance mediatorless microbial fuel cells. Bioresour Technol 114:275–280. https://doi.org/10.1016/j.biortech.2012.02.116

Logan BE (2005) Simultaneous wastewater treatment and biological electricity generation. Water Sci Technol 52(1–2):31–37. https://doi.org/10.2166/wst.2005.0495

Logan BE, Hamelers B, Rozendal R, Schroder U, Keller J, Freguia S, Aelterman P, Verstraete W, Rabaey K (2006) Microbial fuel cells: methodology and technology. Environ Sci Technol 40(17):5181–5192. https://doi.org/10.1021/es0605016

Peng X, Yu H, Yu H, Wang X (2013) Lack of anodic capacitance causes power overshoot in microbial fuel cells. Bioresour Technol 138:353–358. https://doi.org/10.1016/j.biortech.2013.03.187

Potter MC (1911) Electrical effects accompanying the decomposition of organic compounds. P R Soc Lond B-Conta 84(571):260–276. https://doi.org/10.1098/rspb.1911.0073

Rabaey K, Verstraete W (2005) Microbial fuel cells: novel biotechnology for energy generation. Trends Biotechnol 23(6):291–298. https://doi.org/10.1016/j.tibtech.2005.04.008

Ramasamy RP, Ren Z, Mench MM, Regan JM (2008) Impact of initial biofilm growth on the anode impedance of microbial fuel cells. Biotechnol Bioeng 101(1):101–108. https://doi.org/10.1002/bit.21878

Wei J, Liang P, Huang X (2011) Recent progress in electrodes for microbial fuel cells. Bioresour Technol 102(20):9335–9344. https://doi.org/10.1016/j.biortech.2011.07.019

Yang Y, Liu T, Zhu X, Zhang F, Ye D, Liao Q, Li Y (2016) Boosting power density of microbial fuel cells with 3D nitrogen-doped graphene aerogel electrode. Advanced Science 3(8):1600097. https://doi.org/10.1002/advs.201600097

Zhang P-Y, Liu Z-L (2010) Experimental study of the microbial fuel cell internal resistance. J Power Sources 195(24):8013–8018. https://doi.org/10.1016/j.jpowsour.2010.06.062

Zhang YZ, Mo GQ, Li XW, Zhang WD, Zhang JQ, Ye JS, Huang XD, Yu CZ (2011) A graphene modified anode to improve the performance of microbial fuel cells. J Power Sources 196(13):5402–5407. https://doi.org/10.1016/j.jpowsour.2011.02.067

Zhu C, Guo S, Fang Y, Dong S (2010) Reducing sugar: new functional molecules for the green synthesis of graphene nanosheets. ACS Nano 4(4):2429–2437. https://doi.org/10.1021/nn1002387